Chapter 8

Hamiltonian Matrix Structure

8.1 Introduction

In Chapters 2-7, our focus is in analyzing extended embedded ensembles for isolated finite interacting quantum systems. As discussed in Chapter 1, the classical GOE is universally regarded as the model for fluctuation properties of generic chaotic quantum systems. However for a complete statistical description of systems such as nuclei and atoms, as the interactions for these systems are two-body, as already emphasized in the previous chapters, EGOE is expected to be most appropriate. On the other hand, banded random matrix ensembles (BRME) [Wi-55, Wi-57, Ca-90, Ca-93, Fy-91, Fy-92] are also employed by some groups. One can infer the appropriateness of GOE, BRME or EGOE representation, for describing statistical properties, by analyzing eigenvalue densities, strength functions, chaos measures such as information entropy, transition strength distributions, expectation values of operators, level and strength fluctuations and so on [Br-81, Ko-01, Fl-99, Go-01, Go-04]. However, an important question is: is it possible to infer the random matrix structure by directly examining the Hamiltonian matrix itself.

Some of the earlier studies of GOE and EGOE structure of nuclear shell-model Hamiltonian matrices were due to Gervois [Ge-68], French and Wong [Fr-70, Fr-71a, Wo-72] and Bohigas and Flores [Bo-71]. Similarly, for atoms, they were due to Rosenzweig and Porter [Ro-60] and Parikh [Pa-78a]. In many of these studies, the matrix dimensions are quite small (in most cases they are 10-50 dimensional). More recently (in the 90's) there has been renewed interest in examining Hamiltonian ma-

trices in nuclear and atomic examples as it is now possible to construct much larger size matrices and more importantly, because random matrix theory has been well established in the 80's. For example, characteristic features, in terms of GOE and EGOE, of the shell-model Hamiltonian matrix of ^{22}Na, $(J^\pi T) = (2^+0)$ with dimension $d = 307$, were studied by French et al [Fr-88, To-86]. Similarly, Zelevinsky et al analyzed GOE and BRME structure of ^{28}Si, $(J^\pi T) = (2^+0)$ and (0^+0) shell-model Hamiltonian matrices, with $d = 3276$ and 839, respectively [Ze-96]. On the other hand, Flambaum et al [Fl-94, Gr-95] using ls coupling studied, in terms of GOE and BRME, the structure of Hamiltonian matrices of CeI, $J^\pi = 4^\pm$, with dimension $d = 260$ for odd parity and 276 for even parity. Similarly, both ls and jj coupling schemes were investigated for Hamiltonian matrices of CeI, $J^\pi = 4^\pm$; PrI, $J^\pi = 11/2^\pm$, with dimension for PrI being $d = 887$ and 737 for odd and even parities, respectively, by Cummings and collaborators [Cu-01]. Going beyond these studies, our purpose in this chapter is to carry out a comprehensive analysis of the structure of nuclear Hamiltonian matrices, with two shell-model examples (^{22}Na, ^{24}Mg), by employing all the measures, for GOE, BRME and EGOE, that are introduced in the literature at various times. For comparison, we have employed SmI atomic example, as this appears to be, from the past analysis [An-03,An-05], the best atomic example for EGOE. All the results presented in this chapter are published in [Ma-10c].

8.2 Matrix Structure by Visualization

With the advances in computer graphics, it is now possible to visualize the coarse grained structure of the H matrices. Given the many-particle matrix elements H_{ij} (in $J^\pi T$ basis for nuclei and in J^π basis for atoms) one can make a plot of the squares of the matrix elements H_{ij}^2 as a function of (i, j). In general, there are many choices for the indices i. Most commonly employed one for i are the basis states indices defined by the ordering of the basis states as used in the shell-model codes. Note that the Hamiltonian operator is one plus two body, i.e., $H = h(1) + V(2)$ and the basis states used for constructing the H matrix are the eigenstates of the one-body part $[h(1)]$ of H. This exercise has been carried out: (i) for lanthanide atoms CeI and PrI by Flambaum et al [Fl-94] and Cummings et al [Cu-01]; (ii) for the lanthanide atoms NdI, PmI and SmI by Angom and Kota [An-05a]; (iii) for ^{28}Si nucleus by Zelevinsky et al [Ze-96].

Alternatively it is also possible to plot the same as a function of the basis state energies $e_i = H_{ii}$. Physically the basis states indices do not carry any significant information. However the basis state energies e_i's give the location of the corresponding strength functions [see Eq. (8.4.2) ahead] and hence they are more meaningful. This exercise has been carried out for the lanthanide atoms NdI, PmI and SmI by Angom and Kota [An-05]. Following this, for visualization we plot H_{ij} as a function of (e_i, e_j).

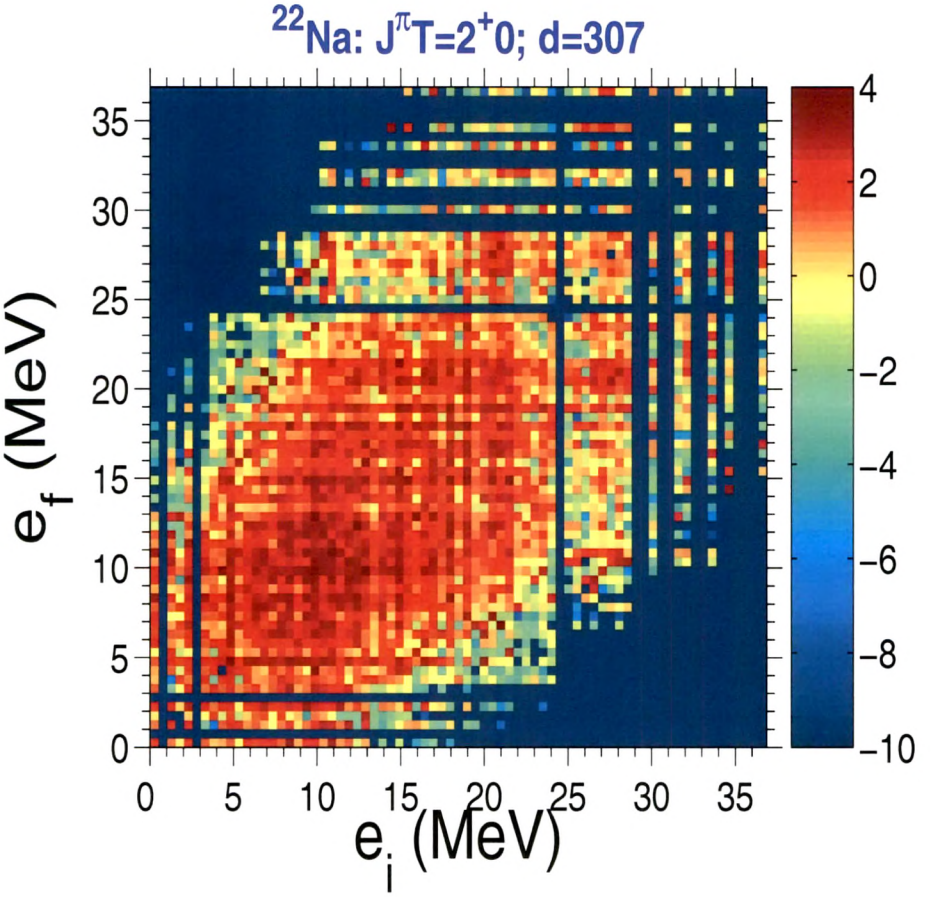

Figure 8.1: Intensity plot showing natural logarithm of the squares of the off-diagonal matrix elements $|\langle f \mid H \mid i \rangle|^2$ (whose value is determined by the color with scale as indicated in the figure) as a function of the single-particle basis state energies $e_i = \langle i \mid H \mid i \rangle$ and $e_f = \langle f \mid H \mid f \rangle$ for ^{22}Na nucleus. Note that diagonal matrix elements $\langle i \mid H \mid i \rangle$ are put to zero in calculating $\sum_{i,f} |\langle f \mid H \mid i \rangle|^2$ in a given bin. Bin-size is 0.5×0.5. All matrix elements are in MeV units and d stands for the matrix dimension. Calculation used Kuo interaction with ^{17}O sp energies; see [Ko-98] for details.

We show in Figs. 8.1 and 8.2 for ^{22}Na ($J^\pi T = 2^+0$, $d = 307$) and ^{24}Mg ($J^\pi T = 0^+0$, $d = 325$) nuclei, respectively, the plot of squares of matrix elements H^2_{kl}, by averaging over an area in the $e_k - e_l$ plane, as a function of the basis state energies (e_k, e_l). For

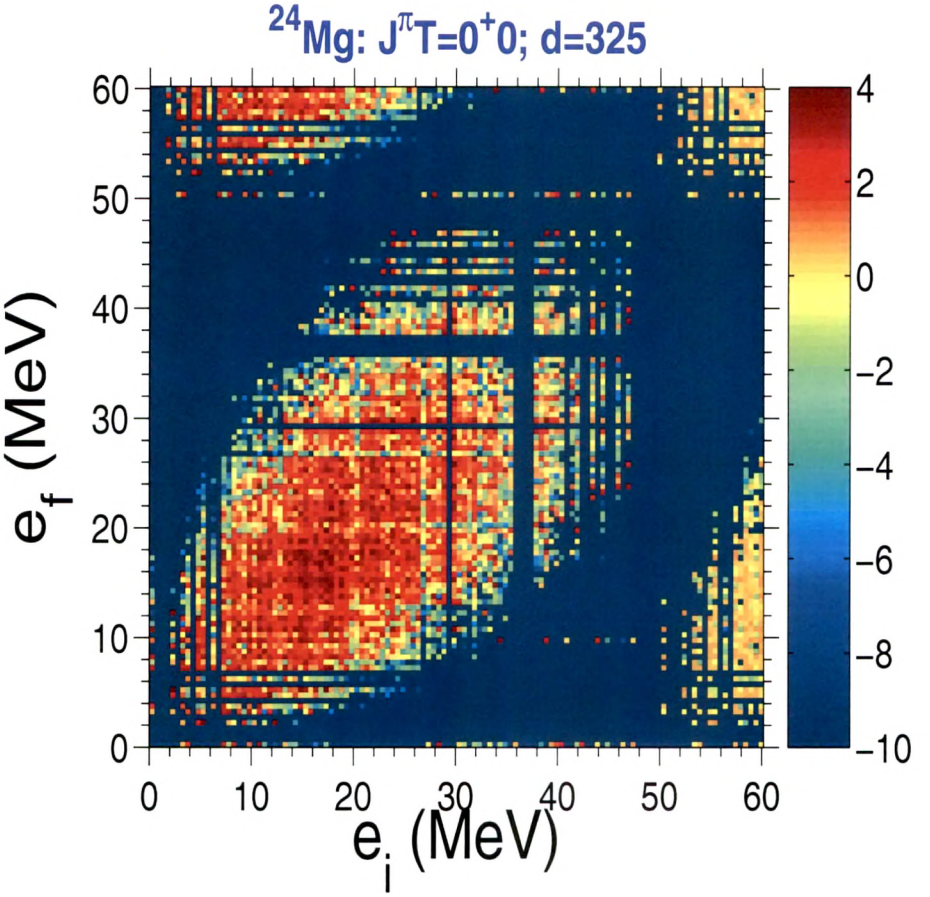

Figure 8.2: Same as Fig. 8.1 but for ^{24}Mg. Bin-size is 0.5×0.5. All matrix elements are in MeV units. Calculation used Kuo interaction with ^{17}O sp energies; see [Ko-02] for details.

details of the nuclear shell-model calculations for ^{22}Na and ^{24}Mg see Refs. [Ko-98] and [Ko-02], respectively. In the plots, we employ a color code for better visualization. Similarly, in Fig. 8.3, H matrix plot for SmI ($J^{\pi} = 4^{+}$, $d = 7325$) atom is shown. Only the first 6300 basis states are taken into consideration in the plot as discussed in Ref. [An-05] and unlike in [An-05], we have used a color code for the plot for better visualization. For ^{22}Na and ^{24}Mg examples, the matrix is more spread compared to that for SmI. This is because, unlike in SmI example (also in many other atomic examples as discussed in [An-05]), in the nuclear shell-model all excitations within the model space are taken into account. Figs. 8.1 and 8.2 show a sparse, band-like structure with block structure within the band. As seen from Fig. 8.3 for SmI H matrix, there are prominent diagonal blocks and streaks of large matrix elements parallel to the diagonal but far away from the diagonal. Also, there is a sparse, band like structure

with block structures within the bands. It is seen from Figs. 8.1, 8.2 and 8.3 that, in general, strictly speaking the H matrices are neither GOE nor banded. Also, from the visualization in Figs. 8.1, 8.2 and 8.3, it is not possible to infer the two-body selection rules which form the basis for EGOE description.

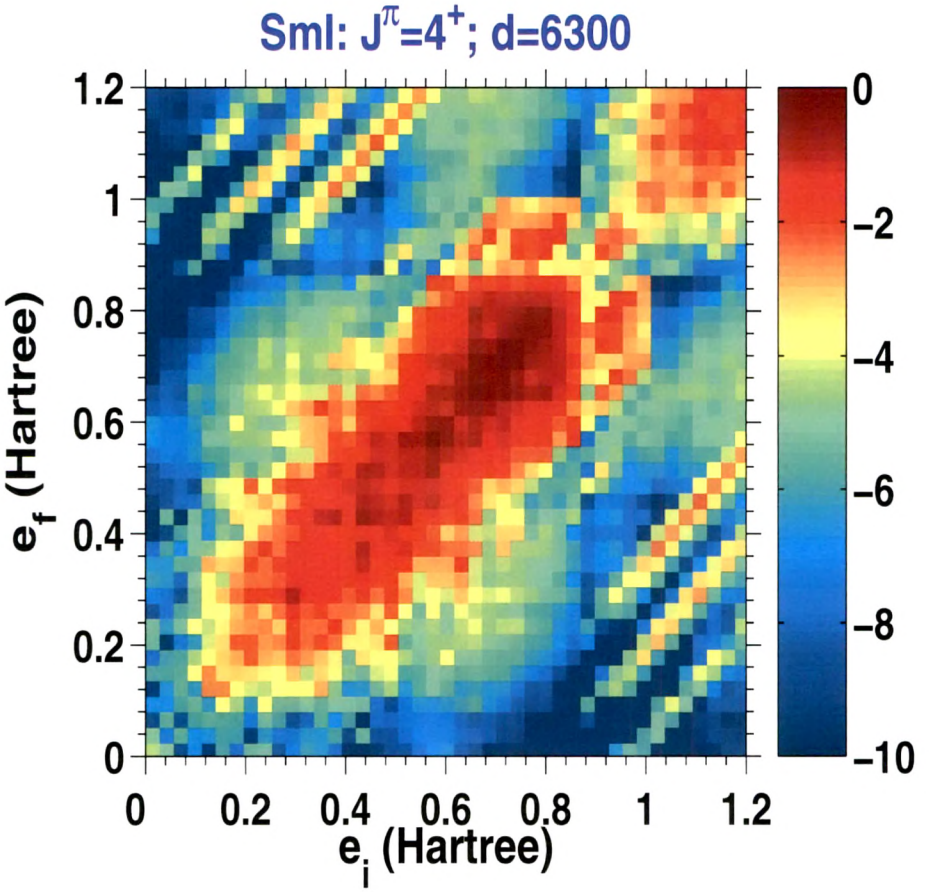

Figure 8.3: Same as Fig. 8.1 but for SmI. The bin-size used is 0.03×0.03. The matrix construction was discussed in [An-05] and these results are used to construct the color plot. Note that all the matrix elements are in Hartree units.

In order to bring out the two-body selection rules clearly, we consider the following representation. In the nuclear shell-model, for m fermions distributed over r sub shells with total angular momentum j_l, $l = 1,2,\ldots,r$, the many-particle states are labeled by the spherical configurations $\mathbf{m} = (m_1, m_2, \ldots, m_r)$, total angular momentum J, isospin T and the multiplicity label α. Note that $m = \sum_{i=1}^{r} m_i$. The m-particle basis states $|\mathbf{m}\alpha JT\rangle$ can be ordered according to the $\mathbf{m}$'s. Then the H matrix will contain diagonal blocks which couple the states within same spherical configuration and off-

diagonal blocks which couple states with different spherical configurations. As the interaction is two-body in nature, there will be only two types of off-diagonal blocks containing non-zero matrix elements which can mix configurations differing in position of one or two particles. All other off-diagonal blocks will contain zero matrix elements. For visual demonstration of this result, we have shown in Chapter 1 in Fig. 1.3, a plot of the H matrix for the ^{24}Mg example displaying the structure due to the two-body selection rules. For this nucleus, there are 8 valence nucleons occupying the three spherical orbits ($1d_{5/2}$, $1d_{3/2}$, $2s_{1/2}$). Therefore the spherical configurations are (m_1, m_2, m_3) with m_1 number of nucleons in $1d_{5/2}$ orbit, m_2 in $1d_{3/2}$ orbit and m_3 in $2s_{1/2}$ orbit. There are 33 configurations generating the 325 dimensional ($J^\pi T = 0^+0$) H matrix. Their dimensions are 35, 34, 28, 27, 23, 20, 19, 15^2, 14, 12, 10, 9^2, 7^2, 5, 4^4, 3, 2^6 and 1^5; here d^n means there are n number of configurations with dimension d. The configurations are ordered such that the block matrices start from the maximum size (35 × 35) and go to the minimum (1 × 1). Figure 1.3 clearly shows the diagonal blocks and the off-diagonal blocks that involve change of occupancy of one and two nucleons, respectively. The regions that correspond to all other off-diagonal blocks are forbidden by the two-body selection rules. A similar figure was given earlier in [Pa-05] for ^{28}Si with $(J^\pi T) = (0^+0)$. Although Fig. 1.3 brings out clearly the structure due to two-body selection rules, it will not give any further insight into the EGOE structure of the matrix. Therefore, for a quantitative understanding of GOE, BRME and EGOE structures of the matrices, we employ various measures introduced in the literature for the structure of these ensembles. Now we will turn to this analysis.

8.3 Analysis in Terms of GOE and BRME

Hamiltonian matrices, prior to the actual diagonalization, are analyzed for the nuclear and atomic examples using measures defining GOE and BRME. To ascertain the GOE character, the distribution of off-diagonal elements is studied. As discussed in Sec. 8.2, the 3D matrix plots show a banded structure. In order to quantify the banded structure, we calculate the bandwidth and the sparsity parameters.

8.3.1 GOE structure: distribution of the off-diagonal matrix elements

Figure 8.4 shows the probability densities $P(x)$ for the off-diagonal matrix elements $x = \widetilde{H}_{kl} = H_{kl}$, $k \neq l$ for ^{22}Na, ^{24}Mg and SmI examples. Figure shows that there are large number of small matrix elements and almost half of these are zeroes. This also implies the leading role of the diagonal matrix elements in forming the spectrum which we will discuss in detail in Sec. 8.4. For GOE, $P(x)$ should be a Gaussian. However, for large $\widetilde{H}_{kl}$, it was found that the distribution $P(x)$ is well described by the Porter-Thomas ($P-T$) distribution [Fl-94],

$$P_{P-T}(x) = \frac{1}{2\sqrt{\pi w|x|}} \exp\left(-\frac{|x|}{w}\right) ; \; x = \widetilde{H}_{kl}, \; w = \sqrt{\overline{\widetilde{H}_{kl}^2}} . \tag{8.3.1}$$

But, the agreement is not good when $\widetilde{H}_{kl} \sim 0$. A better proposition is to use a generalized $P-T$ distribution as suggested first by Zelevinsky et al [Ze-96],

$$P_\kappa(x) = \frac{1}{2}\left[(2x_0)^{\kappa+1}\Gamma(\kappa+1)\right]^{-1} |x|^\kappa \exp\left(-\frac{|x|}{2x_0}\right) . \tag{8.3.2}$$

Note that $x_0 = w/2(\kappa+1)$ and w is given in Eq. (8.3.1). Equation (8.3.2) is found to explain the distribution of the off-diagonal elements in the nuclear examples considered in [Ze-96]. Our examples substantiate this further as discussed below. Note that $\kappa = -1/2$ in Eq. (8.3.2) will give Eq. (8.3.1).

For ^{22}Na, ^{24}Mg and SmI examples that correspond to Figs. 8.1, 8.2, and 8.3, respectively, we have carried out fits to Eq. (8.3.2) with $\kappa = 0, -1/2, -1$ and -2 and found that there is good agreement for $\kappa = -1$ but not for the other values. The fits with $\kappa = -1$ are shown in Fig. 8.4 as continuous curves. In the fits to Eq. (8.3.2), a small region around $x = 0$ is not considered as $P_\kappa(x)$ will not be regular at $x = 0$ for $\kappa \leq -1$. Note that the deviations are larger for SmI example as compared to the nuclear examples. Therefore, our two nuclear examples (to some extent, even the atomic example) are in conformity with the conclusion of Zelevinsky et al. They state [Ze-96]: *Eq. (8.3.2) implies that the normally distributed quantities in the realistic cases are not the off-diagonal matrix elements themselves as would be the case in canonical ran-*

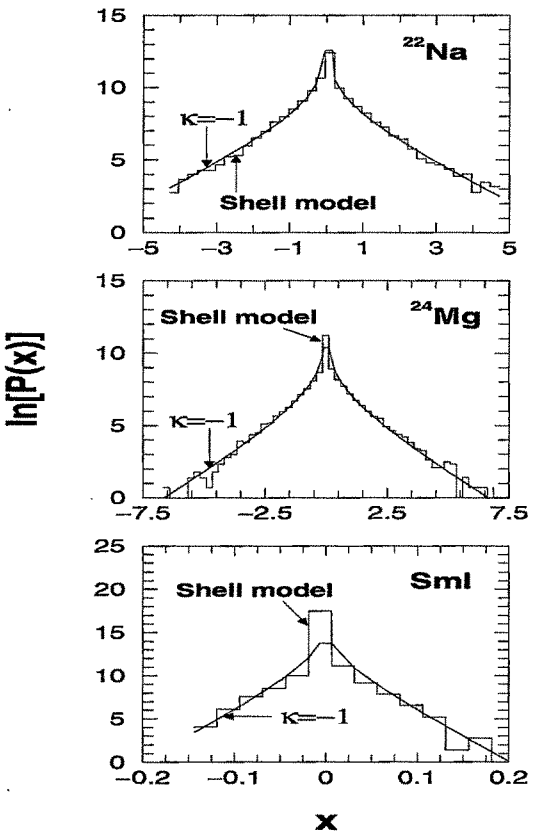

Figure 8.4: Plot showing distribution $P(x)$ of the off-diagonal matrix elements for ^{22}Na, ^{24}Mg and SmI. Note that $P(x)$ gives number of $x = \tilde{H}_{kl}$ in a given energy bin. The bin-size in the figures is 0.25 for ^{22}Na and ^{24}Mg and 0.025 for SmI. In the figure, exact results are shown as histograms and the best fits $P_{\kappa=-1}(x)$ are shown as continuous curves. The function $P(x)$ is normalized to $d(d-1)$, the number of off-diagonal matrix elements. Finally, note that the plots are for $\ln[P(x)]$ vs x. The units for x are MeV for ^{22}Na and ^{24}Mg and Hartree for SmI.

dom matrix ensembles but rather some quantities resembling square roots of them. As they have argued, it is possible that the multipole-multipole form of the nuclear interactions could be the physical reason for this. Hence, it is clear that GOE is not an appropriate representation for the nuclear (also atomic) Hamiltonian matrices.

8.3.2 BRME structure: bandwidths and sparsity

As seen from Figs. 8.1, 8.2 and 8.3, the H matrices have a band-like structure. We calculate a measure for sparsity and also the energy bandwidths for testing the BRME representation for the nuclear and atomic Hamiltonian examples.

Gribankina et al [Gr-95] and Cummings et al [Cu-01] defined the sparsity S as a function of Δ, the difference in the indices of the basis states connected by the Hamil-

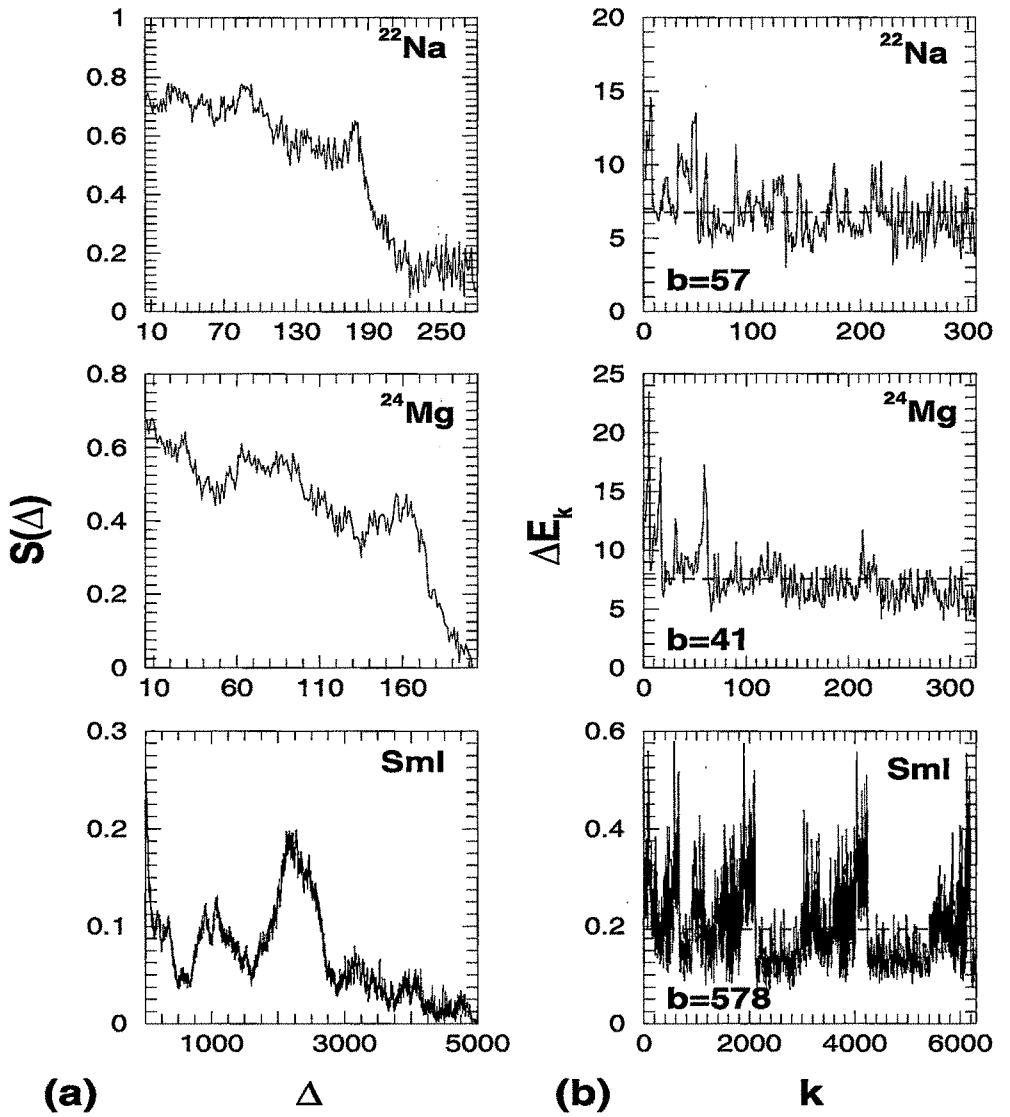

Figure 8.5: (a) Sparsity $S(\Delta)$ defined by Eq. (8.3.3) as a function of $\Delta = |k-l|$ for ^{22}Na, ^{24}Mg and SmI matrices. Results are shown for $\Delta \geq 5$. Note that for calculating sparsity, all the matrix elements whose absolute value is $\geq 10^{-5}$ and 10^{-8}, respectively for the nuclear and atomic examples are taken as non-zero. (b) Energy bandwidths ΔE_k defined by Eq. (8.3.4) as a function of state index k along with mean values of ΔE_k (dashed lines) for ^{22}Na, ^{24}Mg and SmI matrices. The units for ΔE_k are MeV for ^{22}Na and ^{24}Mg and Hartree for SmI. The values of the bandwidths b are shown in the figures.

tonian, as a measure for band-like structure. The definition of S is,

$$S(\Delta) = \frac{\text{number of } |H_{kl}| \neq 0}{\text{number of all } H_{kl}}, \quad |k-l| = \Delta\,. \tag{8.3.3}$$

For a BRME of bandwidth b, the sparsity $S = 1$ for $\Delta \leq b$ and zero for $\Delta > b$, thus it is a step function. Figure 8.5(a) shows the results for $S(\Delta)$ for the three examples ^{22}Na,

^{24}Mg and SmI. In the nuclear examples, $S(\Delta)$ essentially decreases as a function of Δ with approximate linear dependence on Δ up to $\Delta \sim 150$ and then falls sharply to zero. However, there are sizeable fluctuations in S as a function of Δ. On the other hand, for SmI, the structure is quite different with large fluctuations and a peak at $\Delta \sim 2250$. The latter may be due to the large off-diagonal streaks seen in Fig. 8.3. Thus, $S(\Delta)$ shows clear deviation from band-like structure in all the examples. This is further substantiated by the energy bandwidths for the basis states and we will turn to this now.

Energy bandwidth b gives the energy interval in which the basis states are strongly mixed. The energy bandwidths ΔE_k for each basis state k are defined as [Fe-91],

$$\Delta E_k^2 = \frac{\sum_l (H_{kk} - H_{ll})^2 |H_{kl}|^2}{\sum_{l \neq k} |H_{kl}|^2} . \tag{8.3.4}$$

In Fig. 8.5(b) we show the results for ΔE_k for the ^{22}Na, ^{24}Mg and SmI examples. The value of the average bandwidth b is given as the ratio of the mean value of ΔE_k and the mean level spacing of the unperturbed energy levels D, i.e., $b = \overline{\Delta E_k}/D$; in general b can be energy dependent as D can be defined as the local mean spacing of the energy levels. The values of b are given in Fig. 8.5(b) and for all the three examples, b is smaller than the matrix dimension d by a factor of ~ 4. The number b can also be calculated by fitting the mean squared matrix elements to the simple exponential ansatz [Fy-91, Fy-92],

$$\langle H_{kl}^2 \rangle_{|k-l|=\Delta} = H_0^2 \exp\left(-\frac{\Delta}{b}\right) . \tag{8.3.5}$$

The values obtained using Eq. (8.3.5) are almost same as those obtained using Eq. (8.3.4). Significant observation from the figures is as follows. For a BRME, the bandwidth ΔE_k should be independent of k. However, there are significant fluctuations in the energy bandwidths in the nuclear examples and quite large fluctuations in SmI example. Note that it is impossible to reach a banded form even by reordering the basis states and this is due to the two-body selection rules. By combining the results for sparsity $S(\Delta)$ and the energy bandwidths ΔE_k shown in Fig. 8.5, we can conclude that BRME is not a good representation for the H matrices.

8.4 Analysis Using Measures for EGOE Structure

Going further, we analyze three measures for quantifying the EGOE structure of the H matrices for the two nuclear examples and the one atomic example in the present section.

8.4.1 Correlations between diagonal matrix elements and eigenvalues

Large number of numerical calculations in the past in the context of statistical nuclear spectroscopy have clearly indicated [Fr-83, Ko-89] that the joint probability distribution $\rho(E, e_k)$ of the diagonal matrix elements e_k and eigenvalues E is a bivariate Gaussian for EGOE. Therefore the marginal densities $\rho(E)$ and $\rho(e_k)$ will be close to Gaussians with same centroids but different widths. In addition, the widths of the conditional densities $\rho(E|e_k)$ will be independent of e_k. These results were used to derive a formula for the chaos measures, the number of principal components and information entropy in wavefunctions for embedded ensembles [Ko-01a]. The close to Gaussian form of $\rho(E)$ and $\rho(e_k)$ imply that the eigenvalues E and the diagonal elements of the H matrix (or equivalently the basis state energies) will be correlated. Flambaum et al examined, for CeI, eigenvalue spectrum vs the spectrum generated by e_k [Fl-94]. They found a close correlation between the two spectra.

There is recent interest in the topic of correlations between eigenvalues and diagonal matrix elements and several examples from nuclei and also random matrices have been discussed in [Sh-08, Yo-09a]. We show in Figs. 8.6 and 8.7, density of eigenvalues and density of diagonal matrix elements for the Hamiltonian matrices of ^{22}Na, ^{24}Mg and SmI. The distributions are compared with the Gaussian form $\rho_{\mathcal{G}}(\widehat{x})$ and the Edgeworth (ED) corrected Gaussian form $\rho_{ED}(\widehat{x})$; see Eq.(2.3.2) for definitions. Here, $\widehat{x} = (x - x_c)/\sigma$ where x_c is the centroid and σ is the width of the distribution of x. It is clearly seen that the eigenvalue distributions for the two nuclear examples are quite close to $\rho_{\mathcal{G}}(\widehat{x})$ while the densities of the diagonal matrix elements are, with some deviations, close to $\rho_{ED}(\widehat{x})$. However, there are stronger deviations from $\rho_{ED}(\widehat{x})$ for the SmI example, both for the eigenvalue density and the density of the diagonal elements. Here, the eigenvalue density has a secondary peak and the density of diagonal

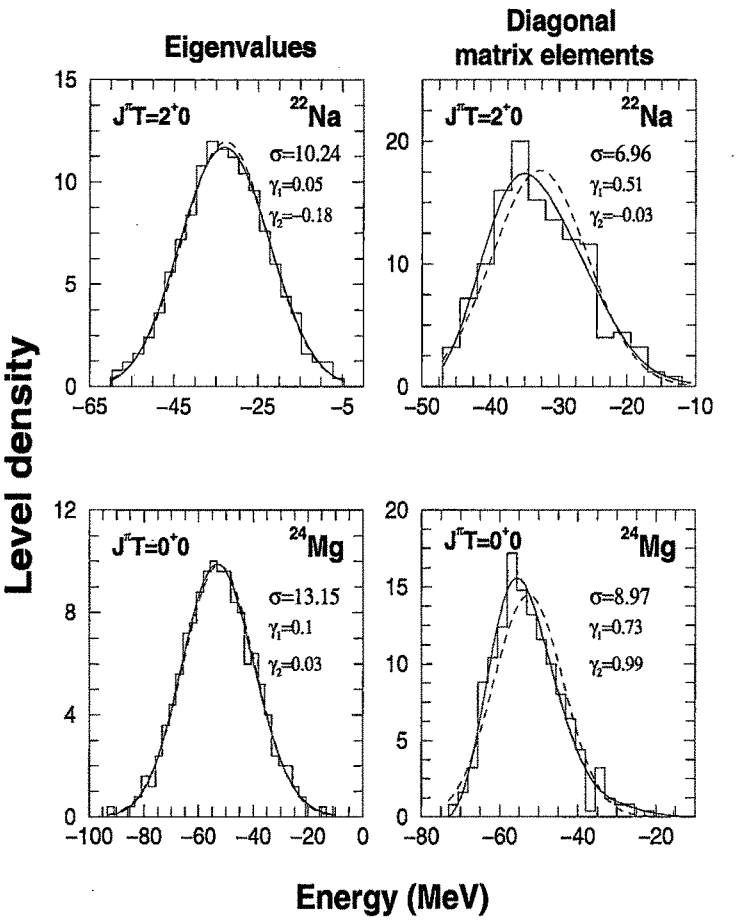

Figure 8.6: Plot showing density of eigenvalues and density of diagonal matrix elements for the Hamiltonian matrices of ^{22}Na and ^{24}Mg. Values of the widths σ, skewness γ_1 and excess γ_2 are given in the figures. The units for σ are MeV. The centroid $E_c = -32.77$ MeV for ^{22}Na and -52.59 MeV for ^{24}Mg. Histograms are the exact results with bin size 2.5 MeV for all the examples. The dashed curves are the Gaussians with centroid E_c given above and width σ whose value is given in the figure. Similarly continuous curves are Edgeworth corrected Gaussians defined in Eq. (2.3.2).

matrix elements displays a stronger bimodal form. Results in Fig. 8.6 reconfirm that in the nuclear examples, the eigenvalues and the diagonal matrix elements of the H matrix are highly correlated and their distributions are close to Gaussian forms. However, there are stronger deviations from this behavior for the SmI example.

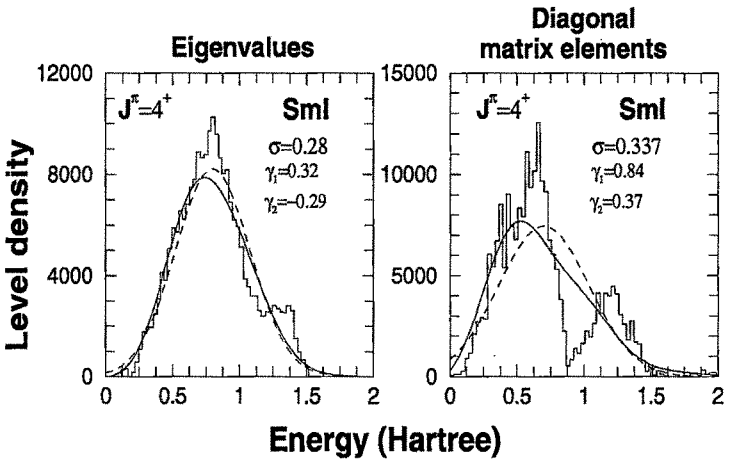

Figure 8.7: Same as Fig. 8.6 but for SmI matrix. The units for σ are Hartree. The centroid is $E_c = 0.7$ Hartree (all energies are given with respect to the lowest energy). Histograms are the exact results with bin size 0.028 Hartree. The eigenvalue density for SmI is constructed by scaling appropriately the data taken from Fig. 3 in [An-05].

8.4.2 Fluctuations in the basis states spreading widths

Going beyond the diagonal matrix elements, it is also useful to consider the basis state widths $\sigma(k)$ where

$$\sigma^2(k) = \langle k \mid H^2 \mid k \rangle - e_k^2 = \sum_{l \neq k} |\langle l \mid H \mid k \rangle|^2 . \tag{8.4.1}$$

It should be noted that $\sigma(k)$ are the widths of the strength functions $F_k(E)$ and similarly e_k are their centroids. Given the mean field $h(1)$ basis states (denoted by $|k\rangle$) expanded in the H eigenvalue (E) basis, $|k\rangle = \sum_E C_k^E |E\rangle$, the strength functions $F_k(E)$ are defined by,

$$F_k(E) = \sum_{E'} \left| C_k^{E'} \right|^2 \delta(E - E') = \left| \mathscr{C}_k^E \right|^2 I(E) . \tag{8.4.2}$$

In Eq. (8.4.2), $\left|\mathscr{C}_k^E\right|^2$ denotes the average of $|C_k^E|^2$ over the eigenstates with the same energy E and all the quantities are defined over good JT (nuclei) or J (atoms) spaces; the strength functions over good spin spaces are also defined in Chapter 2. The strength functions define the spreading of the basis states over the eigenstates and for EGOE the spreadings are of Gaussian form in the strong coupling limit; see [Fr-83, Ko-01] and Chapter 2. Also as stated above, the bivariate Gaussian form of $\rho(E, e_k)$ implies $\sigma^2(k)$ should be constant i.e., they are independent of k. We show in Fig. 8.8,

results for $\sigma(k)$ vs k for ^{22}Na, ^{24}Mg and SmI matrices. It is seen that the basis state widths $\sigma(k)$ are almost constant apart from small fluctuations in the nuclear examples. This result is in agreement with several previous numerical calculations [Ze-96, Fr-83, Ko-08]. Writing $\sigma(k) = \overline{\sigma(k)}(1 \pm \delta)$, it is seen that the relative rms deviation of the fluctuations from the mean values is 14% and 15% (i.e., $\delta = 0.14$ and 0.15, respectively) and the mean values $\overline{\sigma(k)} = 7.5$ MeV and 9.6 MeV, respectively for ^{22}Na and ^{24}Mg matrices. For SmI, $\overline{\sigma(k)} = 0.14$ Hartree and $\delta = 0.25$. Therefore, the fluctuations in $\sigma(k)$ are much larger for SmI as compared to those for the nuclear examples.

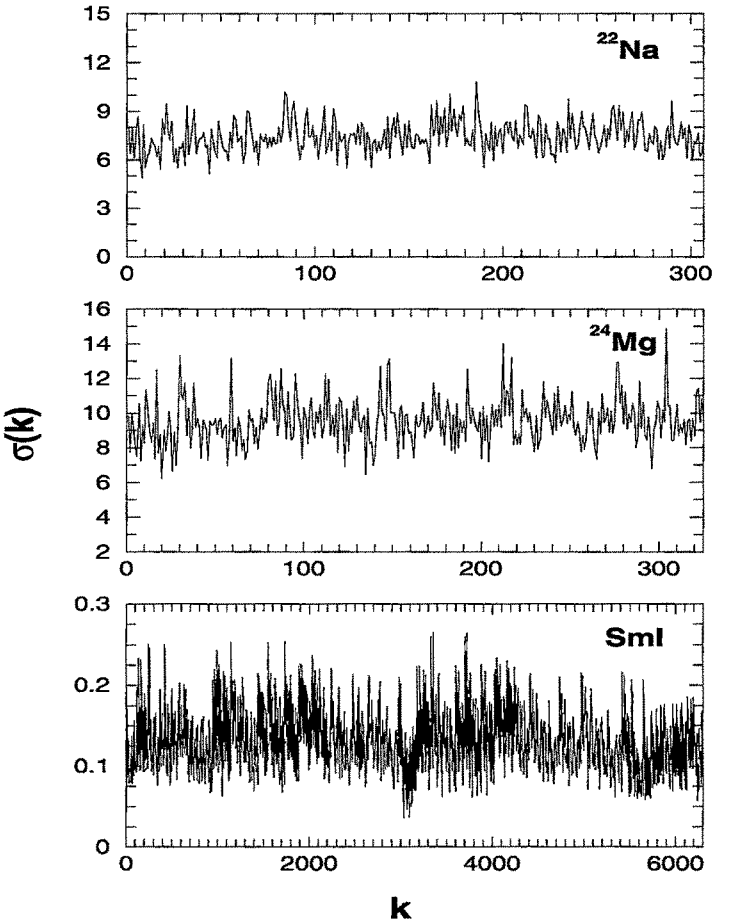

Figure 8.8: Plot showing the variation of width $\sigma(k)$ with the basis state index k for ^{22}Na, ^{24}Mg and SmI matrices. The units for $\sigma(k)$ are MeV for ^{22}Na and ^{24}Mg and Hartree for SmI.

It is possible to estimate the magnitude of the fluctuations in $\sigma(k)$. Say there are K number of many-particle states that are directly coupled by the two-body interaction. The connectivity factor K also defines the spectral variances; see [Fl-96, Fl-96a, Ja-01] and Chapter 2. Assuming that the coupling matrix elements are inde-

pendent Gaussian random variables with zero centroid and variance v^2, we have $\overline{\sigma^2(k)} = v^2K$. Now the relative rms fluctuations in the $\sigma^2(k)$ are given by $\sqrt{2/K}$. Therefore, $\sigma(k) \sim [\,\overline{\sigma^2(k)}\,]^{1/2}(1 \pm 1/\sqrt{2K})$ giving δ defined above to be $1/\sqrt{2K}$. For embedded ensembles for spinless fermion systems with m fermions in N sp states, the connectivity factor $K \sim m(m-1)(N-m)(N-m-1)/4$ [Fl-96, Fl-96a]. For example, for 6 fermions in 12 sp states ($N = 12,\ m = 6$), $\delta \sim 0.05$. Going to embedded ensembles for fermion systems with spin ($\mathbf{s} = \frac{1}{2}$) degree of freedom and assuming that the variances of the matrix elements in the two-particle spin $s = 0$ and $s = 1$ channels to be v_s^2, we can relate v_s to v by demanding that the two-particle spectral variance in both the models is same. This gives $v_s^2 = v^2/4$ for large N. Using this scaling and the result for the connectivity factor $K(S) = K(\Omega, m, S) = P(\Omega, m, S)$ given in Chapter 2, we obtain $\delta \sim 0.1$ for 6 fermions in 6 sp orbits (so that $N = 12$) with total spin $S = 0$. Therefore, going from embedded ensembles for spinless fermion systems to systems with spin, relative rms fluctuations in the basis states variances change from 5% to 10% (see also Table 4.10). We expect the EGOE results for nuclei with JT symmetry to be larger than that of the embedded ensembles for spin systems and this explains the results in Fig. 8.8 for the nuclear examples.

8.4.3 Structure of the two-body part of the Hamiltonian in the eigenvalue basis

In general, it is possible to examine the H matrices in different bases. For example for $(2s1d)$ shell nuclei, the $U(24) \supset [U(6) \supset SU(3) \supset SO_L(3)] \otimes [SU(4) \supset SU_S(2) \otimes SU_T(2)] \supset SO_J(3) \otimes SU_T(2)$ basis [El-58] will be interesting. Similarly, Zuker et al [Zu-01] examined the structure of Lanczos tridiagonal H matrices for nuclei. Unlike examining the total H matrix, it was suggested in [Fr-88] that it may be useful to analyze the pure two-body part $\mathbf{V}$ of H [$\mathbf{V}$ is defined by dropping the diagonal matrix elements of the two-body part $V(2)$] as this part is responsible for chaos (note that the one-body part of H generates Poisson fluctuations). The two natural basis to consider are the shell-model mean-field basis and the H eigenvalue basis. The structure of $\mathbf{V}$ in the mean-field basis is essentially same as that shown in Figs. 8.1, 8.2 and 8.3. Therefore new insight is expected from the structure of $\mathbf{V}$ in the H eigenvalue basis. Unlike the mean-field basis or the $SU(3)$ basis mentioned above (or even any other

basis defined by a group symmetry), the H basis is expected to be the least biased and also it is the most natural basis. More importantly, EGOE has a prediction, as discussed ahead, for the structure of $\mathbf{V}$ in the H basis. As the ^{22}Na nuclear example was discussed before [Fr-88, To-86] and the SmI example showed strong deviations from EGOE structure as discussed in Secs. 8.4.1 and 8.4.2, we restrict our discussion here to ^{24}Mg example.

For ^{24}Mg example, starting with the matrices for $\mathbf{V}$ and H in the mean-field basis [H operator consists of two-body matrix elements due to Kuo [Ku-67] defining $V(2)$ and ^{17}O sp energies -4.15 MeV, 0.93 MeV and -3.28 MeV for $1d_{5/2}$, $1d_{3/2}$ and $2s_{1/2}$ orbits defining $h(1)$] we have constructed the matrix $\langle E_f \,|\, \mathbf{V} \,|\, E_i \rangle$. Using this we have analyzed the bivariate transition strength density generated by the operator $\mathbf{V}$ (we put $\langle E_i \,|\, \mathbf{V} \,|\, E_i \rangle = 0$ as discussed in [Fr-88] so that we are dealing with the pure two-body part of H). Given the transition operator $\mathbf{V}$, transition strength density $I_{\mathbf{V}}^{H,m}(x,y)$ with the two variables x and y being eigenvalues of H is $I_{\mathbf{V}}^{H,m}(x,y) = I^{H,m}(y) |\langle m,y \,|\, \mathbf{V} \,|\, m,x \rangle|^2 I^{H,m}(x)$. The bivariate moments of this distribution are $\widetilde{M_{pq}} = \langle\langle \mathbf{V} H^q \mathbf{V} H^p \rangle\rangle^m$. Note that the normalization factor is M_{00}. Starting with $\widetilde{M}_{pq}$, we can obtain normalized moments, the central moments, reduced moments and also the reduced cumulants k_{rs}, $r+s \geq 3$. It is possible to write down the Edgeworth corrected bivariate Gaussian that includes the cumulants k_{rs} with $r+s = 3,\ 4$ [Fr-88, Ko-95]. Following the spinless EGOE results in [Fr-88, To-86] and the new results in Chapter 7, it can be argued that EGOE gives in general close to bivariate Gaussian form with Edgeworth corrections for $I_{\mathbf{V}}^{H,m}(x,y)$. Equation (J3) in Appendix J gives the bivariate Gaussian form with ED corrections. This prediction of EGOE is tested in Fig. 8.9 for ^{24}Mg. The spectrum span for this nucleus is from -93.29 to -10.06 MeV. The bivariate distribution $I_{\mathbf{V}}$ is shown in Fig. 8.9 and it is constructed using the bin-size 5×5 MeV^2. For comparison, we also show the corresponding ED corrected Gaussian distribution. The marginal centroids ϵ_i, ϵ_f are equal and their value is -50.44 MeV. Similarly, the marginal widths are 13.76 MeV and the bivariate correlation coefficient $\zeta_{biv} = 0.61$ MeV. Thus, it is clear that the matrix can not be represented by a GOE as $\zeta_{biv}^{GOE} = 0$. The bivariate cumulants ($k_{rs} = k_{sr}$ due to symmetry of the $\mathbf{V}$ matrix) for $r+s \leq 4$ are $k_{21} = 0.035$, $k_{30} = 0.070$, $k_{22} = -0.092$, $k_{31} = -0.053$ and $k_{40} = -0.015$. The overall normalization is 12933.25 MeV^2. It is seen from Fig. 8.9 that the r.m.s.

matrix elements of $\mathbf{V}$ in the H eigenvalue basis are well described by the EGOE bivariate Gaussian form. This along with the previous [Fr-88, To-86] ^{22}Na example and all other results in Secs. 8.4.1 and 8.4.2 support the conjecture that EGOE is a good representation for nuclear Hamiltonians.

8.4.4 Comments on deviations from EGOE in the atomic example

Although both the nuclear and atomic shell-model Hamiltonians include a one-body and two-body parts, it is clearly seen that EGOE does not describe very well the atomic shell-model Hamiltonian while it is good for nuclei. Following are some of the differences in the two systems: (i) given the sp orbits and the number of valence fermions, only a few configurations (that correspond to single and double excitations with respect to the leading configuration) are included in atomic calculations [Fl-99, Cu-01, An-05] whereas all configurations allowed in the model space, just as in EGOE, are included in the nuclear examples; (ii) for atoms, both positive and negative parity (interwoven) sp orbits are included (and this is necessary) while in nuclear examples, orbits of only one parity are considered; (iii) the inter-configuration mixing is weak for atoms as discussed in earlier atomic calculations [Fl-99, Cu-01]; (iv) the Coulomb interaction is of long range while nuclear interactions are of short range. A simple plot of the distribution of the configuration centroids with degeneracy given by the dimensions shows multimodal structure for atoms (see Fig. 4 of [An-05]). However, for nuclear examples it is essentially an unimodal distribution and this difference can be ascribed to (i) and (ii). Random matrix model taking into account (i), (ii) and (iii) corresponds to partitioned EGOE [Ko-01]. A simpler version of this model shows that weak mixing between configurations generates bimodal (in general, multimodal) forms for density of states [Ko-99]. Similarly, in order to understand the effects due to (iv), the model considered by Bae et al [Ba-92] may be relevant. This model includes a parameter ξ, where ξ is the ratio of the radius of the many-body system to the range of the interaction. It will be useful to examine the statistical properties considered in the present chapter using both partitioned EGOE and the Bae et al model. However, this analysis is beyond the scope of the present thesis.

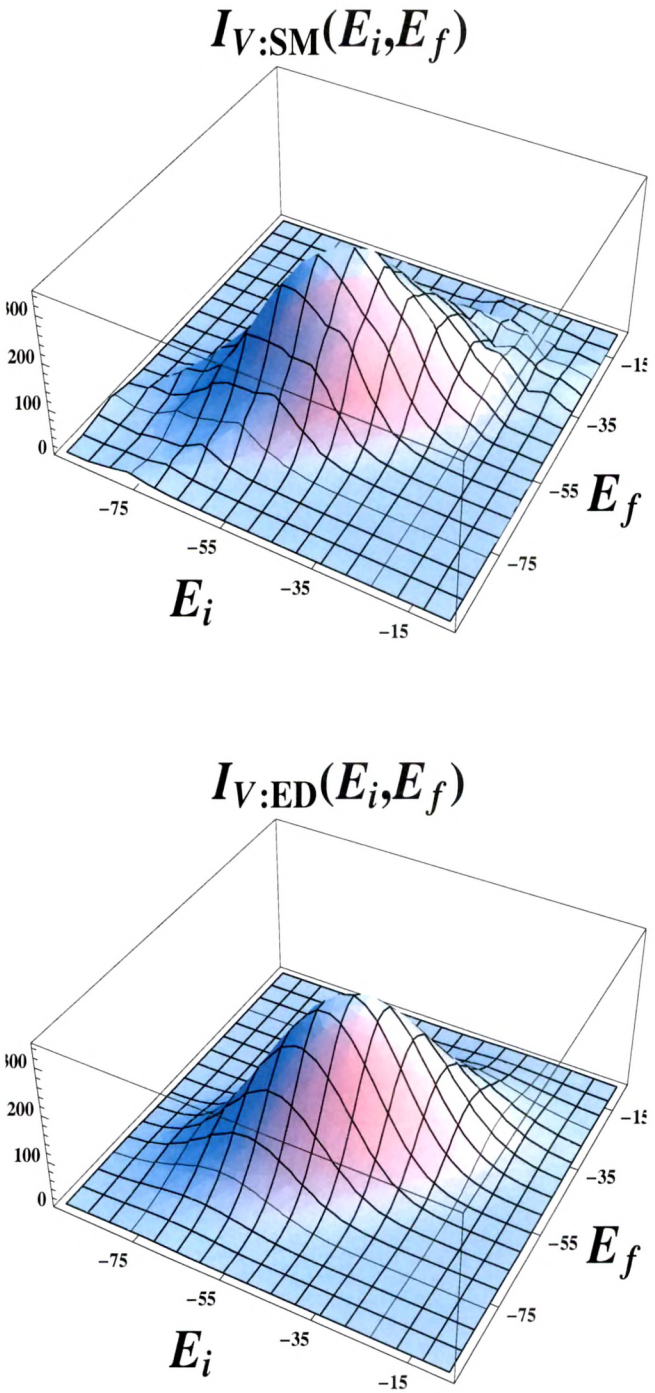

Figure 8.9: Plots showing the bivariate transition strength density for ^{24}Mg with $(J^\pi\, T) = (0^+ 0)$. Compared are the results from exact shell-model (denoted by $I_{\mathrm{V}:SM}$ in the figure) with the Edgeworth corrected bivariate Gaussian $I_{\mathrm{V}:ED}$ in Eq. (J3) obtained using the bivariate cumulants given in the text. The units for E_i and E_f are MeV.

8.5 Summary

In the present chapter, a comprehensive analysis of the structure of nuclear shell-model Hamiltonian matrices has been carried out by employing all available measures for GOE, BRME and EGOE random matrix ensembles. To this end, considered are ^{22}Na and ^{24}Mg nuclear examples and for comparison the SmI atomic example. In the nuclear examples, the matrix sizes are ~ 300 and comparing with some of the analysis carried out by Zelevinsky et al [Ze-96] and Papenbrock and Weidenmüller [Pa-07] where much larger size matrices are used, it is clearly seen from the results in Secs. 8.2-8.4 that the present examples are adequate for bringing out all the essential features of the nuclear shell model Hamiltonians and in particular, the EGOE structure. Results for SmI in Secs. 8.2-8.4 indicate that further investigations are needed for establishing the extent to which EGOE can be applied for describing statistical properties of atomic levels. For nuclear Hamiltonians, it is possible to argue, using chaos measures applied to the diagonal blocks in Fig. 1.3, that there is a local GOE structure (i.e., each diagonal block is close to a GOE with weak admixings between these blocks) in the matrices although there is a global EGOE structure [Pa-05]. This aspect was also recognized in the earlier studies of H matrices by French et al [Fr-88]. The study presented in Secs. 8.2-8.4 together with the previous analysis in [Pa-07, Fr-88, Ze-96] clearly establishes that EGOE is the best random matrix representation for nuclear shell-model Hamiltonians.